Optical properties of epitaxial iron garnet thin films

S. H. Wemple, S. L. Blank, J. A. Seman, and W. A. Biolsi
Bell Laboratories, Murray Hill, New Jersey 07974
(Received 14 June 1973)

Optical absorption, derivative absorption, reflectivity, and derivative reflectivity data are presented for several iron garnet thin-film compositions grown by liquid-phase epitaxy. In the case of yttrium iron garnet (YIG), the real and imaginary parts of the dielectric response function $\epsilon = \epsilon_1 + i\epsilon_2$ are compared with previously published results for bulk crystals and shown to be substantially larger. Based on absorption and reflectivity data for iron garnet films in which the tetrahedral and octahedral iron sublattices have been selectively diluted with gallium or scandium as well as measured absorption data for bulk crystals of yttrium gallium garnet dilutely doped with Fe^{3+}, we propose an Adler-Feinleib split-density-of-states diagram for YIG. The main results include a series of weak crystal-field transitions between 1.4 and 3.4 eV, a pair of much stronger transitions at 2.9 and 3.2 eV which we tentatively associate with excitons of the configuration $2p^5 3d^6$, strong $2p \rightarrow 3d$ charge transfer bands above 3.4 eV where the final states are probably itinerant-one-electron band states, and very strong semiconductor like $2p \rightarrow 4s$ optical transitions above about 8 eV which make the major contributions to the low-frequency refractive index. Some of the above assignments are defended by comparing optical properties of YIG, NiO, and $SrTiO_3$.

I. INTRODUCTION

Recent advances[1] in the growth of high-quality single-crystal iron garnet films by liquid-phase epitaxy (LPE) allow a reexamination[2,3] of the optical properties of these materials, since very thin samples (~1–20 μm) having large (~1 cm^2) as-grown flat surfaces are now available for transmission and reflectance measurements. The iron garnets that concern us in the present study have the general formula $R_3Fe_{5-x}C_xO_{12}$ with 8 formula units per cubic cell. Here R denotes yttrium, a trivalent rare-earth ion, or in some cases a combination of rare-earth ions adding up to 3; while C denotes, for our purposes, either gallium or scandium. These latter substitutions were made in order to selectively alter the fractional site occupancy of the Fe^{3+} ions located in the three distorted tetrahedral sites ($\bar{4}$ local symmetry) per formula unit relative to the two distorted octahedral sites ($\bar{3}$ local symmetry); that is, Ga substitutes preferentially (>90%)[4] for tetrahedral Fe while Sc substitutes preferentially (≈100%)[4] for octahedral Fe. As our prototype iron garnet ($x = 0$) we use $Y_3Fe_5O_{12}$ (YIG), since this material has been studied extensively in the past.

Earlier single-crystal optical-absorption results[5–9] have been largely limited[10] to absorption coefficients below about 2000 cm^{-1} because of sample-thickness limitations inherent in the use of bulk crystals. Wood and Remeika[5] have examined the region of the absorption edge between about 1.0 and 2.4 eV and have related their results to a superposition of crystal field ($3d \rightarrow 3d$ within Fe^{3+}) and charge transfer [oxygen($2p$) → iron($3d$)] transitions, as discussed earlier by Clogston[11] and by Wickersheim and Lefever.[9] They also found[5,8] that optical transmission for photon energies below the "absorption edge" near 1.2 eV could be improved substantially over results of previous studies[6,7] by suitably doping with such tetravalent ions as Si^{4+}, Ge^{4+}, or Sn^{4+}. A series of doping experiments[8] involving both Si^{4+} and Ca^{2+} strongly suggested that the extra absorption tail in the infrared, observed in undoped crystals grown from a PbO-B_2O_3 flux, was related to the presence of Fe^{4+} ions. An examination of Fe^{2+}-Fe^{4+} equilibrium in this system has been given by Nassau.[12]

One of the most interesting observations of Wood and Remeika[5] was the nearly quadratic dependence of the iron-related absorptions in YIG on the total iron content for concentrations above a few atomic percent. This result, as noted by these authors, implies that a simple view of optical transitions involving isolated and atomiclike Fe^{3+} ions cannot be entirely valid. Difficulties associated with interpretation of optical spectra in transition-metal oxides (e.g., NiO) have been noted by many authors.[13,14] It is clear from the energy-band calculations of Mattheiss[15,16] and others that one-electron $3d$-states overlap sufficiently with the relatively broad (~4 eV) oxygen-$2p$ band to form broad Bloch-like $3d$ bands in the usual semiconductor sense. This one-electron picture, while valid for the empty conduction band in, for example, $SrTiO_3$ is no longer valid when the d states become partially filled as in NiO and the iron garnets. In these cases electronic correlations, which are ignored in the one-electron band calculations, become sufficiently important to "condense" the itinerant d electrons into highly correlated localized d states which resemble those of the free ion.[13,17–20] This

localized d-electron model is supported not only by the high resistivity of many transition metal oxides but also by the observation[21] that the many-electron $3d \rightarrow 3d$ crystal-field transitions associated with Ni^{2+} in $Ni_xMg_{1-x}O$ occur at almost precisely the same energies for all values of x. Similarly, many of the Fe^{3+} crystal-field transitions observed in YIG are also observed[5] in yttrium gallium garnet (YGG) dilutely doped with Fe^{3+}.

We may ask how this localized point of view can be made compatible with the observation cited earlier that the strengths of iron-related optical absorptions in YGG: Fe^{3+} increase almost quadratically with iron content. Clearly there are non-localized aspects to the iron $3d$ electrons, but we could have anticipated this result by noting the very large antiferromagnetic Fe(tetrahedral)-O-Fe(octahedral) exchange interaction[22] in YIG. It is also important to recognize that the spin-forbidden (and also parity forbidden in the case of octahedrally located Fe^{3+}) crystal-field transitions are provided with oscillator strength by admixture of nearby, and in some cases overlapping, charge transfer transition of the type oxygen($2p$) $\rightarrow$ iron($3d$). Kahn *et al.*[23] have discussed these transitions in some detail in connection with their polar Kerr effect measurements, using a standard molecular orbital framework based on the earlier work of Clogston.[11] More recently, Wittekoek and Lacklison[24] used this same approach to analyze Faraday rotation spectra in some bismuth iron garnets.

While it is useful in some cases, this molecular-orbital approach fails to draw a clear distinction between band and localized states. To help clarify this important point we make use of the split-density-of-states plot introduced by Adler and Feinleib[13] in their discussion of NiO. One-electron band states are drawn to the left of a vertical line, while many-electron d states, localized by electronic correlation, are drawn to the right. Figure 1 shows a sketch of a possible energy-level scheme for YIG. Superscripts labeling each of the one-electron bands to the left refer to the total available number of electronic states per formula unit. The energy scale is relative, although we expect that the oxygen-$2p$ band is about 4-eV wide,[15,16] that the minimum $2p \rightarrow 4s$ separation is about 6–8 eV, and that the width of the d band is about 3–4 eV.[15,16] We have indicated schematically that four main peaks in the density of states curve can be identified qualitatively with the molecular-orbital states that are important components of the bands in these regions. The e and t_2 states are associated with tetrahedral Fe^{3+}, while the e_g and t_{2g} states refer to octahedral Fe^{3+}. Also, we have taken the usual ordering ($e > t_2$) and ($t_{2g} < e_g$), but the relative energy positions shown are only illustrative at this point. Furthermore, it should be emphasized that these

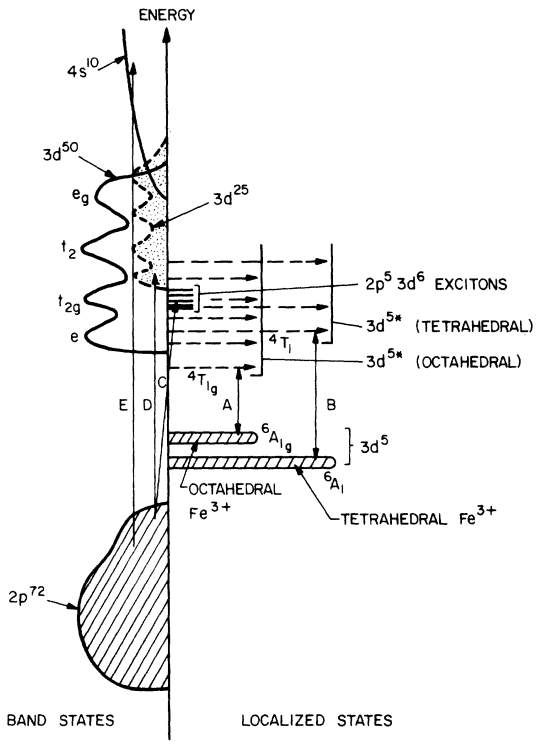

FIG. 1. Proposed Adler-Feinleib energy-level scheme for iron garnets. Band states are shown to the left, and localized states to the right. The superscripts on the bands refer to the number of states per formula unit.

itinerant band states are delocalized and cannot therefore be viewed as quantitatively identifiable with a particular iron sublattice.

As pointed out above, this one-electron-band picture fails to include electron-electron interactions (electronic correlations) which are expected to localize the 25 occupied d states per formula unit. The many-electron ground state of this localized $3d^5$ manifold is shown to the right in Fig. 1. Because these electrons are highly localized, they can be identified separately with either tetrahedral or octahedral sites as indicated in the figure, i.e., of the 25 localized d electrons, 15 are in tetrahedral sites, and 10 are in octahedral sites. Both ground states belong to the configuration $^6A_1$. Their energy positions relative to the band states or to each other cannot be fixed, however, unless optical transitions across the center line can be identified.[13] For this reason no significance should be attached to the relative energies between the two halves of Fig. 1. The excited-state multiplet levels ($3d^{5*}$) shown by the dashed arrows indicate the usual $3d^5$ crystal-field levels. These levels are shown in more detail in Fig. 2, which reproduces the Tanabe and Sugano diagrams[25] for tetrahedral and octahedral Fe^{3+} as given for YIG by Wood and

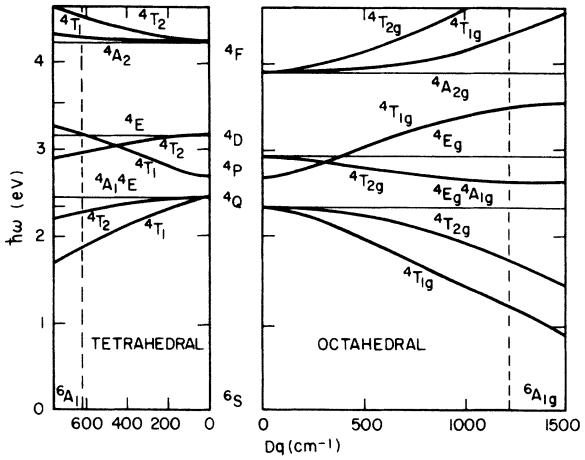

FIG. 2. Energy-level scheme for Fe^{3+} taken from Ref. 5. The vertical dashed lines correspond roughly to crystal-field values in YIG.

Remeika.[5] The vertical dashed lines are reported by these authors as providing the best fit to their spectroscopic data. In Fig. 1 transition A ($^6A_{1g} \rightarrow {}^4T_{1g}$) corresponds to the lowest "band gap" near 1.1 eV (peak near 1.4 eV) in the iron garnets, while transition B ($^6A_1 \rightarrow {}^4T_1$) produces an absorption peak at 2.0 eV. These are weak transitions,[4,5,21] since they are spin forbidden and, in the case of octahedral Fe^{3+}, they are also parity forbidden. As discussed by Kahn *et al.*[23] these forbidden transitions are provided with oscillator strength by spin-orbit interaction and lattice distortions which combine to admix the nearby electric-dipole-allowed $2p \rightarrow 3d$ charge transfer bands.

Electric-dipole-allowed transitions can occur from the filled oxygen-$2p$ band to either the iron-d-electron system or to the broad iron-$4s$ band. In the former case we have indicated a series of localized excitonic levels having the configuration $2p^5 3d^6$ lying just below a continuum of bandlike d states labeled $3d^{25}$. The excitonic states could involve nearest-neighbor or possibly next-nearest-neighbor electron-hole interactions and might even be unresolvable due to electron-phonon broadening. The continuum d band contains half the density of states ($3d^{25}$) when compared with the empty one-electron band discussed earlier ($3d^{50}$), and electronic correlations are assumed to be of minor importance. Optical transitions of the type $2p \rightarrow 3d$ are shown by arrows C and D in Fig. 1. Transitions to localized excitonic d levels were considered by Adler and Feinleib[13] for NiO, but these authors did not include the continuum of bandlike d states in their discussion, and they also placed the $3d^9$ levels at very high energies (>12 eV). The importance of both localized and Bloch d states in transition-metal oxides has been stressed by Ramirez *et al.*[20] in their discussion of metal-insulator transitions. They also suggest that interactions between localized and extended states would make relative energy positions dependent on their respective occupations.

In addition to the $p \rightarrow d$ charge transfer optical transitions noted above, there are electric-dipole-allowed $2p \rightarrow 4s$ transitions indicated by arrow E in Fig. 1 at higher energies. The threshold for such transitions, neglecting exciton formation, would correspond to the band gap in materials without d electrons, such as MgO. Finally, we must consider the possibility of optical transitions from localized $3d^5$ states on the right to bandlike s states on the left ($3d^5 \rightarrow 3d^4 4s$). The analogous transition in NiO ($3d^8 \rightarrow 3d^7 4s$) has been proposed[13] as the source of the relatively strong absorption edge observed near 3.5 eV by Powell and Spicer,[14] but the latter authors express considerable uncertainty as to the validity of this interpretation. Such transitions are expected to be rather weak in view of their basically $d \rightarrow s$ character even though an expected[14] admixture of p-like states would remove this limitation to some unknown degree. In any case, the importance of d(localized) $\rightarrow$ s(band) optical transitions in transition-metal oxides has not yet been established. It is possible that they are often masked by the much stronger dipole-allowed $2p \rightarrow 3d$ charge transfer bands discussed above. Experimental evidence supporting this viewpoint is presented in Sec. IV.

To summarize, the main features of our optical model for YIG include sets of weak crystal-field transitions commencing near 1.4 eV, strong charge transfer ($p \rightarrow d$) optical transitions to bandlike d states (including a possible localized excitonic tail) at higher energies, and strong semiconductorlike $p \rightarrow s$ optical transitions at still-higher energies ($\approx$6–10 eV). Complications associated with this multiplicity of optical transitions are revealed by the polar Kerr effect measurements of Kahn *et al.*[23] as well as by the reflectivity results reported by these authors and also by Grant.[26] Many overlapping optical transitions are observed,[5,23,24] but except for a few of the lower-lying crystal-field transitions, detailed interpretation is largely incomplete. Our purpose in the present paper is to reexamine the optical properties (transmission and reflectance) of the iron garnets by taking advantage of the high-quality[27] LPE films that are now available. Because many closely spaced (and weak) crystal-field absorption lines are observed on a broad (and strong) charge transfer background, we have used the technique of wavelength-derivative spectroscopy to greatly improve resolution of the various absorption and reflectance features. Finally, these results are compared with data for yttri-

um gallium garnet (YGG), dilutely doped with Fe^{3+}, in order to help clarify the identification of band and localized states.

II. EXPERIMENTAL PROCEDURES

Absorption and reflectance results were obtained at room temperature using a double-beam spectrophotometer having a mirrored chopper arrangement combined with electronic multiplexing of sample and reference signals. An electronic servo maintains the reference signal at a near constant level. The electronics is similar to that described by Sell.[28] System noise is limited by photomultiplier shot noise. The signal output is first recorded on a multichannel (256 data point) signal averager and then stored on paper tape. These data are then converted to absorption coefficient using multiple-internal-reflection formulas[29] appropriate to the exact film geometry used, i.e., single-sided or double-sided absorbing films on nonabsorbing gadolinium gallium garnet (GGG) substrates. Small interference effects have been averaged out during data reduction. The required refractive indices were taken from the data of Wemple and Tabor.[30] Reflectance measurements were obtained with an angle of incidence near 10° and a front-surface aluminum reference mirror. All films used for reflectance measurements were sufficiently thick that interference effects due to reflections from the back surface were absent.

We have computed the derivatives $d\alpha/dE$ and $d\ln R/dE$ (where α is the absorption coefficient, R is the reflectivity, and E is the photon energy) on a digital computer using a straightforward five-point differentiating and smoothing program. In agreement with Sell[28] we find that digital differentiation has advantages over wavelength-modulation schemes[31] involving, for example, an oscillating fused-silica refractor plate located just prior to the exit slit. In the context of the present paper, the term "wavelength modulation" refers to digital differentiation of the absolute transmission and reflectance data, which, in every case, have been normalized by a "sample out" baseline. The reflectance data have been adjusted slightly to match the reflectivity in the infrared computed from refractive index data. In the case of YIG the infrared refractive index (2.223) has been obtained by subtracting 0.030 from published data[30] for $Gd_{2.3}Tb_{0.7}Fe_5O_{12}$ (2.253). This small difference between yttrium garnets and rare-earth garnets has been found to apply to a variety of compositions.[32] Refractive indices for other compositions used in the present study were estimated from data given in Ref. 30. It should be borne in mind that small refractive-index uncertainties introduce negligible errors in absorption, provided data above approximitity 50% transmission are discarded.

A Kramers-Kronig (KK) analysis[33] of the YIG reflectivity results was performed in order to obtain the real and imaginary parts of the dielectric response function $\epsilon = \epsilon_1 + i\epsilon_2$. Data above $h\nu = 5$ eV were taken from Grant's results, but scaled so as to match exactly our considerably higher reflectance values below 5 eV. A reflectance value at $h\nu = 10$ eV was adjusted to preclude unphysical negative values of ϵ_2 below $h\nu = 2.5$ eV. As a check on the above procedure we found a close match between the ϵ_2 curves obtained at lower energies from the KK analysis and those determined directly from optical-absorption measurements using very thin films (~1 μm thick).

III. EXPERIMENTAL RESULTS

Figure 3 shows the absorption edge of YIG as obtained from direct absorption measurments on films of various thicknesses between 1 and 16 μm and from a KK analysis of reflectance data above 3 eV. The onset of the first octahedral Fe^{3+} crystal-field transition ($^6A_{1g} \rightarrow {}^4T_{1g}$) near 1.1 eV (peak at 1.37 eV) forms the absorption threshold for this material. Other structure is clearly evident at higher energies with the absorption saturating near $\alpha = 5 \times 10^5$ cm^{-1} above 5 eV. As discussed by Wood and Remeika[5] the shoulder at 1.8 eV is the $^6A_{1g} \rightarrow {}^4T_{2g}$ octahedral Fe^{3+} crystal-field transition (see Fig. 2), and the peak at 2.0 eV is the lowest energy $^6A_1 \rightarrow {}^4T_1$ tetrahedral Fe^{3+} crystal-field transition. The higher strength of this transition is presumably due to removal of the parity constraint.[5,10,23]

In Fig. 4 we show the reflectivity results for YIG. Absolute reflectivities are several percent

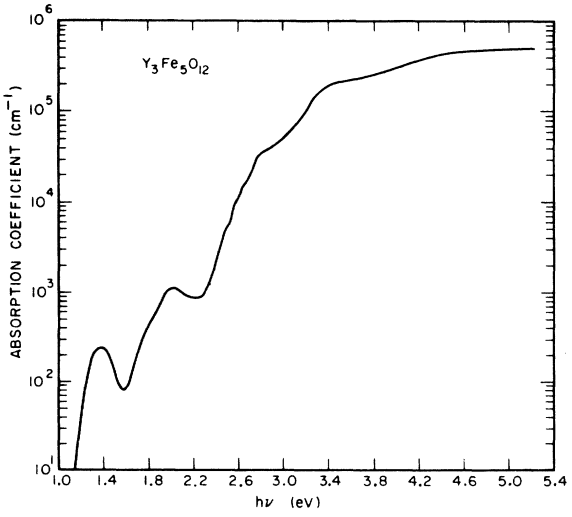

FIG. 3. Absorption edge of YIG obtained from transmission data below 3.1 eV using both LPE films on GGG and bulk crystals and from Kramers-Kronig analysis of reflectance data on thick LPE films above 3 eV.

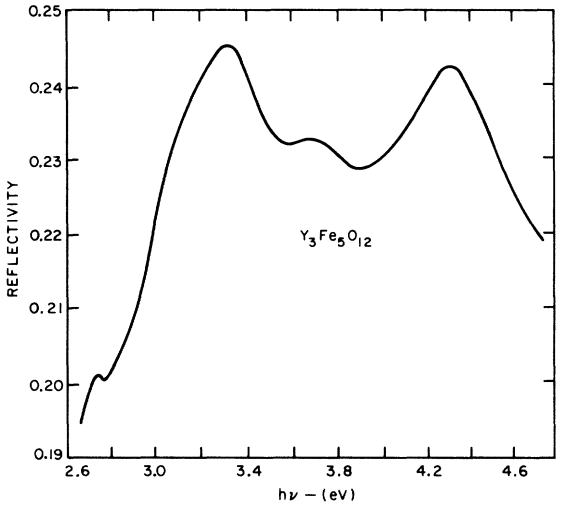

FIG. 4. Reflectivity of YIG.

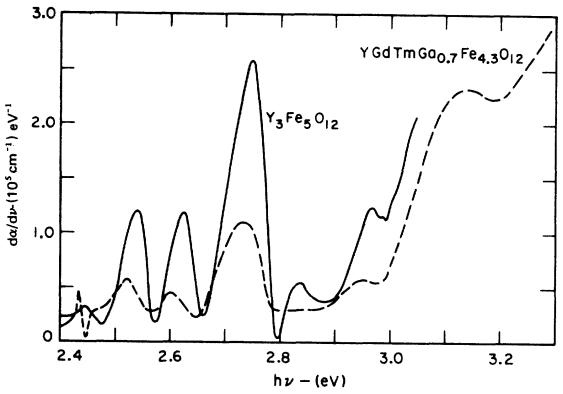

FIG. 6. Derivative absorption results for YIG and $YGdTmGa_{0.7}Fe_{4.3}O_{12}$.

higher than reported by Grant[26] for bulk material, although the observed structural features are essentially the same. Results of a KK analysis combined with direct absorption measurements below 3.1 eV are presented in Fig. 5. As noted earlier we have forced ϵ_1 to fit the known refractive index at low energies and have scaled the reflectivity data of Grant[26] to fit our results above 5 eV. A more detailed discussion is deferred to Sec. IV; however, it should be noted that the magnitudes of both ϵ_1 and ϵ_2 are everywhere considerably higher than reported by Grant. In order to accentuate the weak structure apparent between 2.4 and 3.0 eV in the absorption curve of Fig. 3, we have calculated the absorption derivative shown in Fig. 6. At least six spectral features are clearly evident with a particularly strong one occuring near 2.75 eV. The logarithmic derivative of the YIG reflectivity is given in Fig. 7. Here again considerable structure is revealed by the derivative plot that is not readily apparent in the straight reflectivity data.

In addition to examining the optical properties of YIG, we have studied iron garnet compositions in

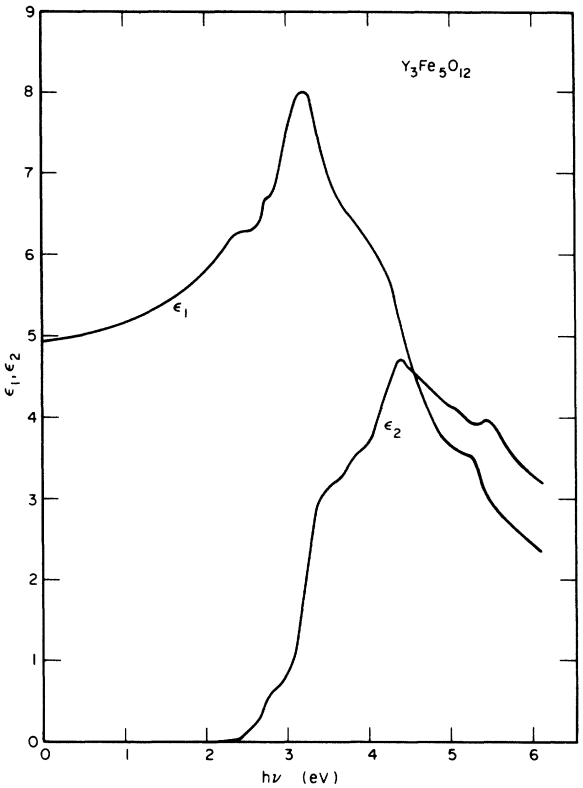

FIG. 5. Real and imaginary parts of the dielectric function $\epsilon = \epsilon_1 + i\epsilon_2$ for YIG.

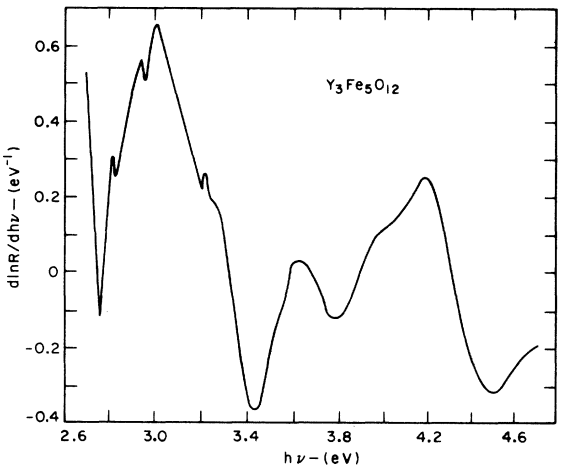

FIG. 7. Logarithmic derivative of the reflectivity for YIG.

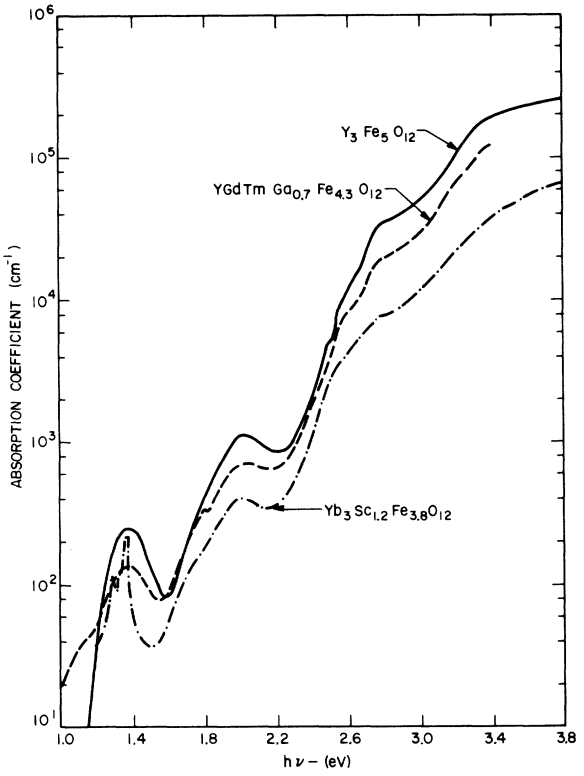

FIG. 8. Absorption edge results for three iron garnets.

which the iron sublattice has been diluted with either Ga^{3+} or Sc^{3+}. In the former case tetrahedral iron is removed, while in the latter case octahedral iron is removed. Absorption results for two such diluted systems are shown in Fig. 8. The weak structure at 1.8 eV in $YGdTmGa_{0.7}Fe_{4.3}O_{12}$ is due

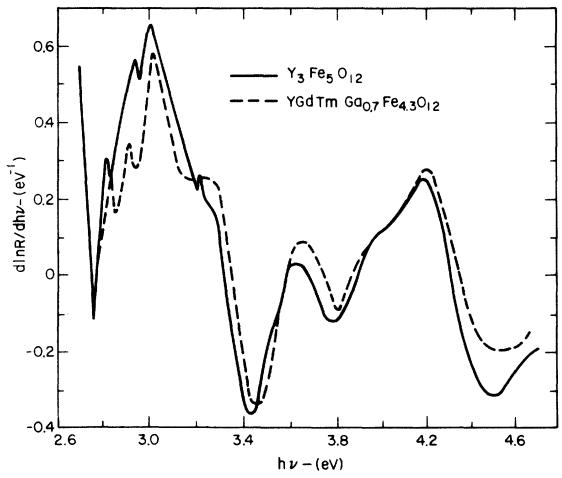

FIG. 9. Logarithmic derivative of the reflectivity for $YGdTmGa_{0.7}Fe_{4.3}O_{12}$ compared with YIG.

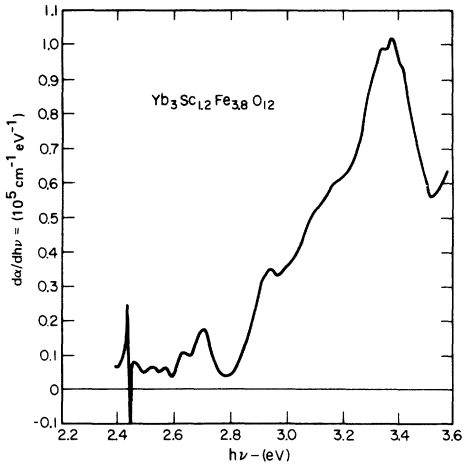

FIG. 10. Derivative absorption results for $Yb_3Sc_{1.2}Fe_{3.8}O_{12}$.

to Tm^{3+}, and the structure near 1.3 eV in $Yb_3Sc_{1.2}Fe_{3.8}O_{12}$ is due to Yb^{3+}. According to Fig. 8 there is, at all energies, a general trend of reduced absorption with iron dilution in either the tetrahedral or octahedral sublattices. The derivative absorption result for $YGdTmGa_{0.7}Fe_{4.3}O_{12}$ is shown by the dashed curve in Fig. 6. The main structural features are the same as in YIG but with intensity reduced by a factor of 2 to 3. Structure in the derivative reflectivity curve for the gallium-substituted garnet is shown by the dashed line in Fig. 9. A pronounced change in the derivative absorption spectrum is produced by large scandium substitutions, as revealed by the derivative plot of Fig. 10. No reflectivity data were obtained for this material.

In order to aid in the interpretation of the foregoing experimental results, we have also measured the absorption spectrum of bulk yttrium gallium garnet (YGG) doped with about 6.2-at.% Fe^{3+}. The experimental results are shown in Fig. 11. Although not shown, there is an additional weak peak near 1.3 eV ($^6A_{1g} \rightarrow {}^4T_{2g}$) having a maximum absorption coefficient of about 0.5 cm^{-1}. Arrows on the figure point to structural features extracted from a computer fit to the absorption derivative results shown in Fig. 12. In both Figs. 11 and 12 the lengths of each arrow correspond to the integrated oscillator strengths of the various spectral lines. The calculated derivative curve in Fig. 12 was determined by a computer fit to a series of overlapping damped Lorentzian absorption lines, using a combined steepest-decent nonlinear least-squares-fitting program. Line positions, strengths, and widths were all adjustable parameters for each resonance. Note that 17 lines can be resolved. Earlier absorption results of Wood and Remieka[5] on

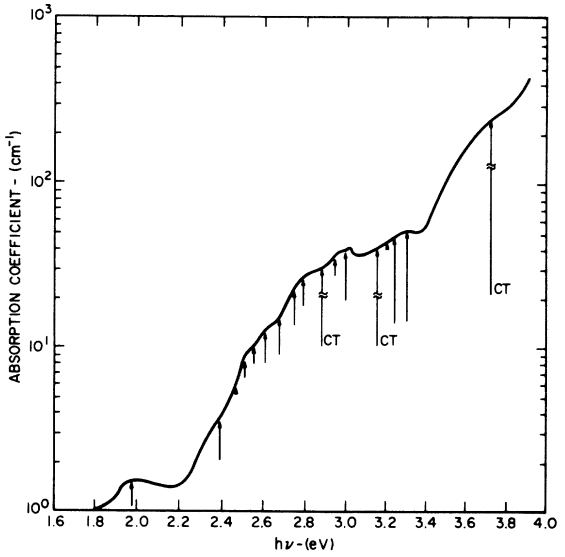

FIG. 11. Absorption coefficient vs photon energy for yttrium gallium garnet doped with 6.2-at.% Fe^{3+}. The arrows give positions and strengths of oscillators that fit the data. CT refers to charge transfer. All other transitions are crystal-field transitions within the $3d^5$ manifold.

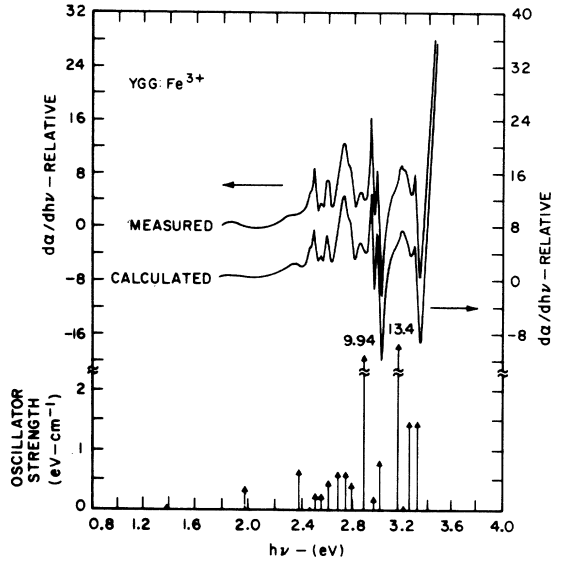

FIG. 12. Derivative absorption results for yttrium gallium garnet doped with 6.2-at.% Fe^{3+}. The calculated curve corresponds to the multiple-damped oscillator fit described in the text and presented at the bottom of the figure.

YGG: Fe^{3+} showed only five spectral lines so that the experimental advantages of derivative spectroscopy are clearly evident. Table I shows the linewidths and integrated strengths for each of the 17 observed lines. The proposed identification is discussed in the following section.

IV. DISCUSSION

In this section we relate the experimental results just presented to the proposed energy-level scheme of Fig. 1. As noted earlier, the presence of both octahedral and tetrahedral Fe^{3+} sites enormously complicates structure assignments, so that some of our conclusions will, naturally, be tentative. As discussed in some detail by Wood and Remeika,[5] the first three absorption peaks in Fig. 3 at 1.37, 1.8, and 2.0 eV are crystal-field transitions within the Fe^{3+} $3d^5$ manifold. According to Fig. 2 the first two transitions ($^6A_{1g} \rightarrow {}^4T_{1g}$ and $^6A_{1g} \rightarrow {}^4T_{2g}$) are associated with octahedral iron while the stronger one ($^6A_1 \rightarrow {}^4T_1$) is associated with tetrahedral iron. The larger strength of the 2.0-eV transition is presumably due to removal of the parity constraint for tetrahedral iron.[5,10,23] As expected, all three of these transitions also occur in YGG: Fe^{3+}. Note, for example, the 2-eV absorption in Fig. 11. Figure 3 shows that there is a rapid increase in absorption above 2.2 eV on which some weak structure is evident. This structure is more clearly revealed by the derivative spectrum of Fig. 6.

Comparison with the YGG: Fe^{3+} derivative spectrum of Fig. 12 reveals an almost one-to-one correspondence up to 2.9 eV, although the dilute system exhibits some fine structure that is not resolvable in YIG, and there appear to be some relatively

TABLE I. Observed low-energy optical transitions in YGG: Fe^{3+}. Identification refers to crystal-field octahedral (CFO), crystal-field tetrahedral (CFT), and charge transfer (CT). FWHM denotes full width at half-maximum.

Position (eV)	FWHM (eV)	Strength (eV cm^{-1})	Identification
1.3	0.13	0.061	CFO
1.77	...	...	CFO
1.98	0.34	0.41	CFT
2.39	0.23	0.68	CFT
2.46	0.036	0.01	CFO
2.51	0.074	0.28	CFT
2.55	0.080	0.26	CFT
2.61	0.092	0.49	CFT
2.68	0.15	0.65	CFT
2.75	0.097	0.62	CFT
2.79	0.087	0.47	CFT
2.88	0.31	9.94	CT
2.96	0.044	0.24	CFT
3.00	0.072	0.84	CFT
3.16	0.42	13.4	CT
3.20	0.081	0.07	CFO
3.24	0.14	1.58	CFT
3.31	0.11	1.58	CFT

minor shifts in energy (transitions occur about 80 meV higher in YIG). Thus we can conclude that all of these transitions involve localized rather than bandlike states. Furthermore, we note from Table I and Fig. 12 that the integrated oscillator strengths of all but one of the transitions between 2.39 and 2.97 eV are within a factor of 2 of the 2-eV crystal-field transition known to be associated with tetrahedral iron.[4] We consequently assign these seven transitions to the tetrahedral Fe^{3+} system. The much weaker transition at 2.46 eV is assigned to the octahedral iron-$3d^5$ multiplet. It is possible, of course, that other octahedral Fe^{3+} crystal-field transitions are present over this spectral region, but they could easily be masked by much stronger tetrahedral iron absorptions.

Returning to the energy-level diagram of Fig. 2 we would suggest that the eleven tetrahedral iron crystal-field transitions observed in YGG: Fe^{3+} between 2.3 and 3.4 eV are associated with transitions ${}^6A_1 \rightarrow {}^4T_2$, ${}^4A_1$, ${}^4E$, ${}^4T_2$, ${}^4T_1$, ${}^4E$. These transitions would be split into at least eleven lines in $\bar{4}$ symmetry. The single octahedral iron transition at 2.46 eV is probably one component of the ${}^6A_{1g} \rightarrow {}^4E$, ${}^4A_{1g}$ doublet. The other component may be masked by stronger overlapping tetrahedral iron transitions. A weak, and presumably octahedral, iron line is also observed at 3.20 eV. This may be a component of the ${}^6A_{1g} \rightarrow {}^4T_{2g}$ doublet. Two transitions observed in YGG: Fe^{3+} at 2.88 and 3.16 eV are an order of magnitude stronger and much broader than all the tetrahedral iron crystal-field transitions just discussed. Note that the strong 2.88-eV line (shifted slightly upward) is also present in the YIG data of Fig. 6, while the 3.16-eV line is clearly present in the Ga^{3+}-substituted composition. Both the 2.88- and 3.16-eV absorptions are evident also in the YIG ϵ_2 data of Fig. 5 and in the YIG reflectivity data of Fig. 4. Because these relatively strong transitions occur in the dilute system and are much stronger than the crystal-field transitions, we tentatively assign them to *localized* $2p \rightarrow 3d$ charge transfer excitons.

Further evidence for this charge transfer assignment is provided by the YIG photoconductivity results of Grant and Ruppel,[34] which show a "threshold" near 2.2 eV followed by rapidly increasing photoconductivity. Unequivocal assignment of these charge transfer excitons to a specific iron sublattice does not appear possible, however, as revealed by the Ga^{3+}- and Sc^{3+}-substituted garnet data of Figs. 6 and 8. Note that *all* transitions are reduced substantially in intensity including the tetrahedral iron crystal-field absorptions. As suggested by Wood and Remeika,[5] this result implies that the charge transfer bands contributing to the oscillator strength of "forbidden" crystal-field transitions involve both the octahedral iron and tetrahedral iron sublattices, e.g., Fe(octahedral)-O-Fe(tetrahedral) molecular complexes or even one-electron charge transfer bands. Similarly, the strong 2.88- and 3.16-eV transitions are both reduced in intensity independent of which iron sublattice is diluted. This is a somewhat puzzling result in view of their presence in the YGG: Fe^{3+} crystal. It should be noted also that the probability is exceedingly small that a given oxygen atom has both its neighboring octahedral site *and* neighboring tetrahedral site filled with an iron atom. The experimental data would suggest perhaps, that the iron atoms in the dilute system tend to group together into Fe-O-Fe complexes rather than be distributed randomly throughout all the available octahedral and tetrahedral sites. In this case we would assign the 2.88- and 3.16-eV absorptions, in either the dilute system or in YIG, to charge transfer excitons involving *both* tetrahedral and octahedral iron atoms associated with each exchange coupled Fe(tetrahedral)-O-Fe(octahedral) complex.

At energies above 3.2 eV the absorption coefficient of YIG increases rapidly according to Fig. 3 and approaches 5×10^5 cm^{-1} above 5 eV. Furthermore, considerable structure is revealed by the reflectivity data of Fig. 4, the ϵ_2 data of Fig. 5, and the derivative reflectivity data of Fig. 7. It is of interest to compare the derivative reflectance results for YIG with recent measurements[35] near 3.4 eV in Si as shown in Fig. 13. The important point is that the reflectance structure in YIG is comparable in both magnitude and width with the Si results, lending support to the view that band-to-band transitions are involved.

Additional evidence for bandlike states is provided in Fig. 14, where we have compared ϵ_2 curves for YIG, $SrTiO_3$,[36] and NiO.[14] In the case of $SrTiO_3$ it is known that bandlike $2p \rightarrow 3d$ charge transfer transitions determine ϵ_2 in this spectral region and that there are $\frac{10}{3}$ empty d states per oxygen atom. In the case of YIG there are $\frac{25}{12}$ empty one-electron d states, and in NiO there are 2 empty d states per oxygen atom. If the same types of $p \rightarrow d$ optical transitions are dominant in all three materials, then the simplest model would yield ratios of oscillator strengths of $1 : \frac{5}{8} : \frac{3}{5}$ for $SrTiO_3$, YIG and NiO, respectively. As a rough guide to the total oscillator strength, we take the area under each ϵ_2 curve to 6 eV and find that the strengths are approximately in the above ratio. This result suggests that one-electron $2p \rightarrow 3d$ charge transfer transitions are dominant in all three materials and that the absorption edge near 3.5 eV observed in NiO is due to such transition rather than to $3d \rightarrow 4s$ electron-promotion transitions as suggested by Adler and Feinleib.[14] Comparison of these materials on the basis of absorption coefficient again reveals striking similarities, as shown in Fig. 15, with satura-

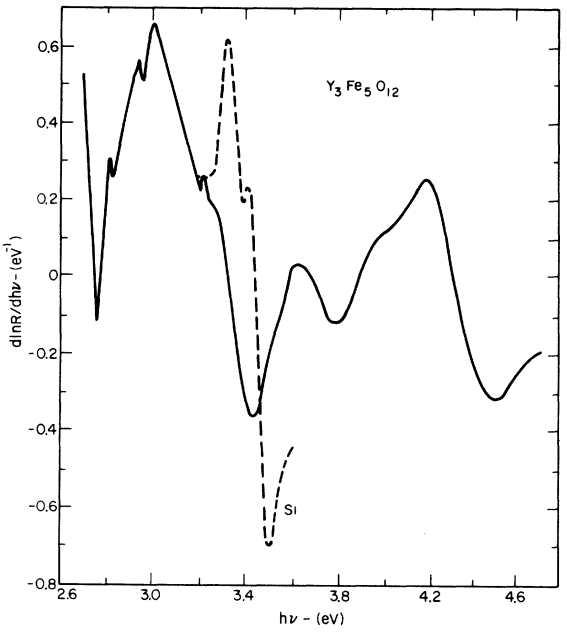

FIG. 13. Comparison of logarithmic derivative results for YIG with structure in Si taken from Ref. 35.

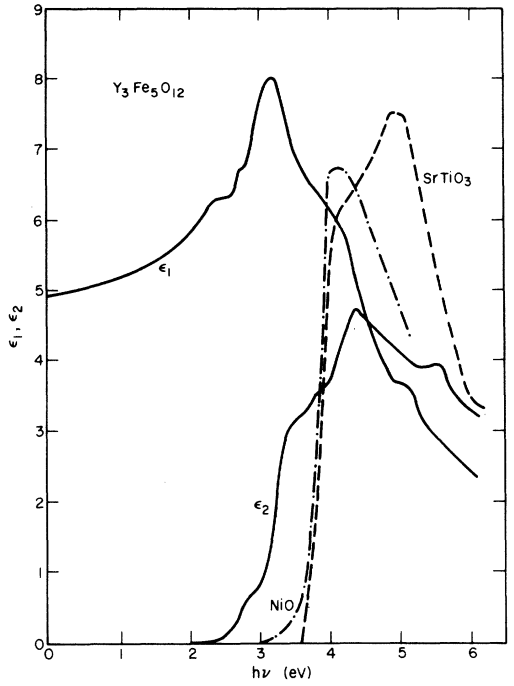

FIG. 14. Comparison of dielectric response functions for YIG, NiO (Ref. 14), and $SrTiO_3$ (Ref. 36).

tion above 5 eV occurring at $(5-8)\times10^5$ cm^{-1}.

At energies above 9 eV Powell and Spicer[14] have observed that the absorption coefficient in NiO increases to near 2×10^6 cm^{-1}, a value typical for dipole-allowed $p \rightarrow s$ interband transitions in semiconductors. This high-energy absorption was therefore assigned to band-to-band $O(2p) \rightarrow Ni(4s)$ transitions. That a similar high-absorption region occurs in YIG can be shown using the refractive-index analysis of Wemple and Tabor.[30] These authors show that the long-wavelengths optical dielectric constant ϵ in $Gd_{2.3}Tb_{0.7}Fe_5O_{12}$ can be decomposed into three terms in the form $\epsilon = 5.1 = 1 + 1.5 + 2.6$, where the first term is the vacuum contribution, the second term is associated with an oscillator near 4 eV, and the final term is associated with an oscillator near 8 eV. We assign the 4-eV oscillator to the $2p \rightarrow 3d$ charge transfer bands. If there were no d electrons present, then the refractive index would be equal to $\sqrt{3.6} = 1.9$, which is close to the index of garnets not containing iron.[30] An estimate of the absorption coefficients required to produce this index can be made using the well-known sum rule[37]:

$$n - 1 = \frac{1}{2\pi^2} \int_0^{\lambda_t} \alpha \, d\lambda , \qquad (1)$$

where α is the absorption coefficient, and the integration extends over the full wavelength interval 0 to λ_t. Equation (1) can be rewritten in terms of the average absorption coefficient $\bar{\alpha}$, in the form

$$n \approx 1 + 6.3\bar{\alpha}/E_t , \qquad (2)$$

where $\bar{\alpha}$ is in units of 10^6 cm^{-1}, and E_t is the approximate photon energy in eV at which the absorption saturates. Taking $n = 1.9$ and $E_t \cong 8$ eV yields $\bar{\alpha} \approx 10^6$ cm^{-1}. Because the true absorption coefficient falls off at very high energies, the peak absorption coefficient is certainly higher than the

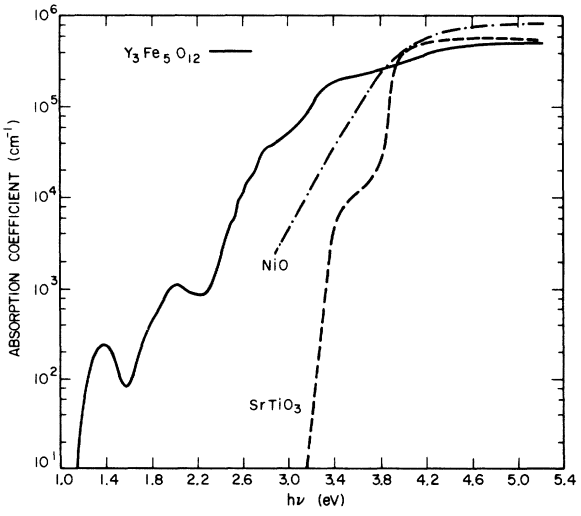

FIG. 15. Comparison of absorption edges in YIG, NiO (Ref. 14), and $SrTiO_3$ [Ref. 36; M. Capizzi and A. Frova. Nuovo Cimento B 5, 181 (1971)].

above average and could easily reach 2×10^6 cm^{-1} as observed[14] in NiO. We conclude that very strong absorptions occur at energies above those shown in Figs. 3 and 5 for YIG, and that these absorptions generally contribute more to the refractive index in garnets than all the optical transitions that involve d electrons. We also suggest that these high-energy absorptions are primarily dipole-allowed $2p \rightarrow 4s$ interband transitions.

V. CONCLUSIONS

The main results of the experimental investigation can be summarized as follows:

(i) A series of Fe^{3+} crystal-field transitions lying between 1.4 and 3.4 eV involve localized d-electron states that can be associated with either octahedral or tetrahedral iron. The number of observed transitions is greatly reduced in the filled lattice (YIG) when compared with the dilute system (YGG: Fe^{3+}), possibly due to a combination of line broadening and masking of the weak octahedral Fe^{3+} crystal-field transitions by the much stronger tetrahedral Fe^{3+} transitions. The strengths of *all* crystal-field transitions decrease with dilution of either tetrahedral iron (with Ga^{3+}) or octahedral iron (with Sc^{3+}) sublattices.

(ii) Optical transitions having strengths more than a factor of 10 above the tetrahedral iron crystal-field transitions are observed at 2.9 and 3.2 eV in both the filled and dilute lattices. We have suggested that these transitions involve charge transfer excitons of the configuration $2p^5 3d^6$. Results for the Ga^{3+}- and Sc^{3+}-substituted systems indicate that these features can not be separately identified with either the octahedral or tetrahedral sublattices. We suggest instead that exchange coupled Fe-O-Fe complexes are involved in keeping with an earlier suggestion of Wood and Remeika.[5]

(iii) Strong optical absorptions above 3.4 eV have been associated with $2p \rightarrow 3d$ charge transfer bands for which the final states are itinerant one-electron band states. This conclusion is based on the widths and strengths of derivative reflectance spectra and the similarities between ϵ_2 and absorption spectra of YIG, $SrTiO_3$, and NiO.

(iv) Very strong semiconductorlike optical transitions occur above about 8 eV. These transitions, which make the major contribution to the refractive index, almost certainly involve $2p \rightarrow 4s$ transitions between the oxygen-$2p$ band and the Fe^{3+} $4s$ band.

Note added in proof. Some recent work has been reported that is directly relevant to the contents of the present paper. Optical absorption data for YIG are contained in N. Wettling, B. Andlauer, P. Koidl, J. Schneider, and W. Tolksdork, Phys. Status Solidi B 59, 63 (1973). An optical study of both YIG and YGG: Fe^{3+}, including a multiple oscillator fit to YGG: Fe^{3+} absorption data, has been submitted by G. B. Scott, D. E. Lacklison, and J. L. Page. These authors have emphasized a crystal-field analysis of observed absorption spectra.

ACKNOWLEDGMENTS

The authors thank L. F. Mattheiss and C. Herring for several informative discussions, and L. G. Van Uitert for the YGG: Fe^{3+} samples.

[1]S. L. Blank and J. W. Nielsen, J. Cryst. Growth 17, 302 (1973).
[2]A preliminary account of this work was presented at The First International Conference on Modulation Spectroscopy, November 23–26, 1972, Tucson, Ariz. (unpublished). See also S. H. Wemple Surf. Sci. 37, 297 (1973).
[3]K. W. Blazey, AIP Conf. Proc., No. 10, 735 (1972).
[4]M. A. Gilleo and S. Geller, Phys. Rev. 110, 73 (1958).
[5]D. L. Wood and J. P. Remeika, J. Appl. Phys. 38, 1038 (1967).
[6]J. F. Dillon, Jr., J. Phys. Radium 20, 374 (1959).
[7]P. Bailey and A. Goldman, Westinghouse Research Laboratories Report (unpublished).
[8]D. L. Wood and J. P. Remeika, J. Appl. Phys. 37, 1232 (1966).
[9]K. A. Wickersheim and R. A. Lefever, J. Chem. Phys. 36, 844 (1962).
[10]Although some absorption data extending above 2000 cm^{-1} have been reported [cf. R. E. MacDonald and J. W. Beck, J. Appl. Phys. 40, 1429 (1969)] the required thin-film samples were either polycrystalline or of uncertain structure due to poor lattice match with the substrate.
[11]A. M. Clogston, J. Appl. Phys. 31, 198S (1960).
[12]K. Nassau, J. Cryst. Growth 2, 215 (1968).
[13]D. Adler and J. Feinleib, Phys. Rev. B 2, 3112 (1970).
[14]R. J. Powell and W. E. Spicer, Phys. Rev. B 2, 2182 (1970).
[15]L. F. Mattheiss, Phys. Rev. B 5, 290 (1972); Phys. Rev. B 5, 306 (1972).
[16]L. F. Mattheiss, Phys. Rev. B 6, 4718 (1972).
[17]D. Adler, in *Solid State Physics*, edited by F. Seitz, D. Turnbull, and H. Ehrenreich (Academic, New York, 1968).
[18]N. F. Mott, Proc. Phys. Soc. A 62, 416 (1949).
[19]J. Hubbard, Proc. Roy. Soc. A 276, 238 (1963).
[20]R. Ramirez, L. M. Falicov, and J. C. Kimball, Phys. Rev. B 2, 3383 (1970).
[21]D. Reiner and Ber. Bunserges, Phys. Chem. 69, 82 (1965).
[22]S. Geller and M. A. Gilleo, J. Phys. Chem. Solids, 3, 30 (1957).
[23]F. J. Kahn, P. S. Pershan, and J. P. Remeika, Phys. Rev. 186, 891 (1969).
[24]S. Wittekoek and D. E. Lacklison, Phys. Rev. Lett. 28, 740 (1972).
[25]Y. Tanabe and S. Sugano, J. Phys. Soc. Jap. 11, 864 (1956).
[26]P. M. Grant, Appl. Phys. Lett. 11, 166 (1967).

[27]Although LPE garnet films are known to contain lead incorporated from the flux, it is unlikely that measured ϵ_1 and ϵ_2 spectra would be affected by such contaminants except, as noted earlier, in the tail region below the absorption edge. For the low-absorption region (<100 cm^{-1}) we have used data obtained from bulk crystals [cf. S. H. Wemple, J. F. Dillon, Jr., L. G. Van Uitert, and W. H. Grodkiewicz, Appl. Phys. Lett. 22, 331 (1973)].

[28]D. D. Sell, Appl. Opt. 9, 1926 (1970).

[29]S. H. Wemple and J. A. Seman, Appl. Optics 12, 2977 (1973).

[30]S. H. Wemple and W. J. Tabor, J. Appl. Phys. 44, 1395 (1973).

[31]See, for example, M. Cardona, *Modulation Spectroscopy* (Academic, New York, 1969).

[32]L. K. Shick, C. D. Brandle, Jr., S. L. Blank, and M. A. Karr, J. Elec. Mat. 2, 609 (1973).

[33]We thank A. S. Barker, Jr. for the Kramers-Kronig program.

[34]P. M. Grant and W. Ruppel, Solid State Commun. 5, 543 (1967).

[35]F. H. Pollak and G. W. Rublaff, Phys. Rev. Lett. 29, 789 (1972).

[36]M. Cardona, Phys. Rev. 140, A651 (1965).

[37]T. S. Moss, *Optical Properties of Semiconductors* (Butterworths, London, 1961), p. 27.